

High-Resolution Cloud Removal with Multi-Modal and Multi-Resolution Data Fusion: A New Baseline and Benchmark

Fang Xu^{a,b}, Yilei Shi^c, Patrick Ebel^b, Wen Yang^a and Xiao Xiang Zhu^b

^aSchool of Electronic Information, Wuhan University, Wuhan, 430072, China

^bData Science in Earth Observation, Technical University of Munich, Munich, 80333, Germany

^cRemote Sensing Technology, Technical University of Munich, Munich, 80333, Germany

ARTICLE INFO

Keywords:

Cloud removal

Data fusion

ABSTRACT

In this paper, we introduce Planet-CR, a benchmark dataset for high-resolution cloud removal with multi-modal and multi-resolution data fusion. Planet-CR is the first public dataset for cloud removal to feature globally sampled high resolution optical observations, in combination with paired radar measurements as well as pixel-level land cover annotations. It provides solid basis for exhaustive evaluation in terms of generating visually pleasing textures and semantically meaningful structures. With this dataset, we consider the problem of cloud removal in high resolution optical remote sensing imagery by integrating multi-modal and multi-resolution information. Existing multi-modal data fusion based methods, which assume the image pairs are aligned pixel-to-pixel, are hence not appropriate for this problem. To this end, we design a new baseline named Align-CR to perform the low-resolution SAR image guided high-resolution optical image cloud removal. It implicitly aligns the multi-modal and multi-resolution data during the reconstruction process to promote the cloud removal performance. The experimental results demonstrate that the proposed Align-CR method gives the best performance in both visual recovery quality and semantic recovery quality. The project is available at <https://github.com/zhu-xlab/Planet-CR>, and hope this will inspire future research.

1. Introduction

Remote sensing imagery has been receiving considerable attention as major promising prospects in various applications such as Earth observation and environmental monitoring (Xia et al., 2018; Yuan et al., 2020; Requena-Mesa et al., 2021; Xiong et al., 2022). However, haze and clouds in the atmosphere affect the transmission of electromagnetic signals and lead to a deficiency of surface information (Duan and Li, 2020), severely hindering the potential of remote sensing imagery. Cloud removal aims at reconstructing the cloud-contaminated regions to counteract the degradations caused by clouds, and thus becomes an indispensable pre-processing step in the analysis of remote sensing imagery. As a continuing concern within the remote sensing community, many exciting progresses on this task have been extensively reported, including many data-driven approaches using deep learning (Ebel et al., 2020; Xu et al., 2022; Cresson et al., 2022). Benefiting from the open access policy of the Landsat program and the Copernicus program, several datasets have been proposed to promote the development of deep learning in the field of cloud removal, like RICE-II (Lin et al., 2019) and SEN12MS-CR (Ebel et al., 2020) datasets. However, there are still two major issues that seriously limit the development of cloud removal:

- *Unavailability of high resolution imagery for existing datasets.* Recent advances in remote sensing have

given rise to the next-generation satellites that provide optical imagery with superior spatial resolution (Kondmann et al., 2021; Cornebise et al., 2022). Such data allows geometric analysis on a finer scale, while posing new challenges for recovering cloud-covered regions with corresponding level of details. The existing datasets with relatively low spatial resolutions severely restrict the development of cloud removal algorithms for recovering clear edge and rich texture details of high resolution remote sensing imagery.

- *Lack of evaluation in generating semantically meaningful structures.* High-quality reconstructed cloud-free images require both visually pleasing textures and semantically meaningful structures. Existing work almost exclusively evaluates the quality of the reconstructed images through image quality metrics like PSNR and SSIM, i.e. evaluates the quality of the reconstructed image in terms of generating visually pleasing textures. While it is desirable to evaluate the semantically meaningful structures to identify the usability of the reconstructed images.

In this paper, we build a *Planet-CR* dataset to fulfill the requirement of high resolution cloud removal datasets. High resolution remote sensing imagery with extensive spatial-temporal coverage is not easily available. Some satellites offer very high resolution imagery only from specific locations, which makes it impractical to construct datasets with a high diversity of globally distributed sites. By trading off the spatial-temporal coverage and the resolution of satellite imagery, we collect data from Planet satellite imagery (PBC, 2018–). Planet provides global daily data

 xufang@whu.edu.cn (F. Xu); yilei.shi@tum.de (Y. Shi); patrick.ebel@tum.de (P. Ebel); yangwen@whu.edu.cn (W. Yang); xiaoxiang.zhu@tum.de (X.X. Zhu)

ORCID(s):

with a spatial resolution of $3m$. On the one hand, it allows to acquire paired cloudy and cloud-free images with a very short temporal offset. It could minimize surface changes that may appear between the acquisitions of cloudy and cloud-free images, thereby minimizing nuisances between cloudy reference images and cloud-free target images. On the other hand, it allows to acquire heterogeneous earth observation data to encourage general-purpose cloud removal but not along narrowly-defined and geo-spatially distinct regions of interest. Meanwhile, the Planet-CR dataset collects corresponding pixel-level land cover annotations from WorldCover product (Zanaga et al., 2021). It offers the chance of validating the effectiveness of the cloud removal methods in generating semantically meaningful structures on a well-established remote sensing task.

Cloud removal is a highly ill-posed problem due to the loss of surface information. Previous studies have reported that the ill-posedness can be reduced by resorting to Synthetic Aperture Radar (SAR) data, which is cloud-penetrable and inherently reflects the geometrical shapes of ground objects (Ebel et al., 2020; Gao et al., 2020; Xu et al., 2022). However, SAR data is usually unaffordable (Atwood and Garron, 2013), especially for global Earth data. Thanks to the freely accessible global SAR data provided by the European Space Agency, we further include the Sentinel-1 SAR data in our Planet-CR dataset to promote cloud removal of PlanetScope data. Compared with the existing cloud removal datasets like SEN12MS-CR, which mostly explore the fusion of Sentinel-1 SAR data and Sentinel-2 optical data with the same resolution of $10m$, our Planet-CR dataset helps to understand a more practical yet more complex problem, i.e. multi-modal and multi-resolution data fusion based cloud removal, in which the misalignment due to resolution difference, field-of-view mismatch, disparity, etc. has to be considered.

To address the problem of multi-modal and multi-resolution data fusion based cloud removal, we propose a novel method called Align-CR, where the low-resolution SAR images guide the reconstruction of high-resolution cloud-free images from cloudy images. Specifically, Align-CR implicitly aligns the feature maps using the deformable convolution (Dai et al., 2017) to compensate for the misalignment between the multi-modal and multi-resolution data. Based on the Planet-CR dataset, we benchmark representative cloud removal methods, and analyze their performance in generating visually pleasing textures by image reconstruction metrics and in generating semantically meaningful structures by a well-established semantic segmentation task. Extensive evaluation demonstrates that the Align-CR method achieves the best performance on the vast majority of our benchmark tests. In summary, our contributions are as follows:

- We construct a dataset Planet-CR collected specially for cloud removal to advance the field, which is the public dataset with the highest spatial resolution to date. It comprises a large number of regions all around

the world with auxiliary SAR imagery and land cover information.

- We propose a novel cloud removal algorithm, Align-CR, which can better capture the correlations across the multi-modal and multi-resolution data to reconstruct the occluded regions.
- We benchmark state-of-the-art cloud removal algorithms with the Planet-CR dataset, which can be used as the baseline for future algorithm development, and conduct extensive evaluations for recovered semantic information on a well-established semantic segmentation task.

2. Related Work

2.1. Datasets for Cloud Removal

To promote the progress of deep learning-based cloud removal, several datasets for cloud removal have been proposed. We provide an overview of publicly available cloud removal datasets, as shown in Tab. 1. RICE-I (Lin et al., 2019) contains 500 pairs of cloudy and cloud-free images collected on Google Earth by setting whether to display the cloud layer, which only contains filmy, partly-transparent clouds. RICE-II (Lin et al., 2019) contains about 700 paired images derived from the Landsat 8 OLI/TIRS dataset, where the acquisition time of cloudy and cloud-free images at the same location is less than 15 days. However, the size of both datasets is relatively small, and the data in them is geographically and topographically homogeneous. STGAN (Sarukkai et al., 2020) contains nearly 100,000 paired Sentinel-2 images drawn from 17800 distinct tiles worldwide. The cloud cover for each cloudy image is between 10% and 30%. It excludes the images with insufficient visible ground upon manual inspection. Then SEN12MS-CR (Ebel et al., 2020) collects around 150,000 samples, containing different types of real-life clouds, from 169 non-overlapping AOIs sampled across all inhabited continents during all meteorological seasons. Each AOI is composed of a pair of orthorectified, geo-referenced cloudy and cloud-free Sentinel-2 images. And to develop cloud removal models that are robust to extensive cloud coverage conditions, each AOI contains an additional co-registered Sentinel-1 SAR image. The related SEN12MS-CR-TS dataset (Ebel et al., 2022) is structured likewise, while featuring multi-season repeated measurements. However, a common limitation of the aforementioned datasets is that they are not stratified by land cover types, making it impossible to assess the generalizability of cloud removal methods over individual land cover type that may be of interest to specific applications like vegetation monitoring (Rogan et al., 2002; Lima et al., 2019; Ngadze et al., 2020) and water resources monitoring (Fisher et al., 2016). To evaluate the effectiveness of cloud removal methods over different land cover types, WHU2-CR (Li et al., 2021) selects 36 locations from all over the world according to three main land covers: urban, vegetation, and bare land, and produces about 20,000 pairs of cloudy and cloud-free Sentinel-2 images. And Czernawski et al. (2022) construct a cloud removal dataset specially in the context

Table 1

Comparison between Planet-CR and existing publicly available cloud removal datasets. LC is short for land cover map.

Dataset	source	Optical Image				w/ SAR	w/ LC
		resolution	#AOIs	width	#images		
RICE-I (Lin et al., 2019)	Google Earth	< 15m	/	512	500	✗	✗
RICE-II (Lin et al., 2019)	Landsat-8	30m	/	512	450	✗	✗
STGAN (Sarukkai et al., 2020)	Sentinel-2	10m	17,800	256	97,640	✗	✗
SEN12MS-CR (Ebel et al., 2020)	Sentinel-2	10m	169	256	122,218	✓	✗
SEN12MS-CR-TS (Ebel et al., 2022)	Sentinel-2	10m	53	256	15,578	✓	✗
WHUS2-CR (Li et al., 2021)	Sentinel-2	10m	36	256	17,182	✗	✗
Scotland&India* (Cerkawski et al., 2022)	Sentinel-2	10m	445	256	445	✓	✗
Planet-CR	PlanetScope	3m	780	300	63,000	✓	✓

* The cloudy observations in the dataset are simulated.

of crop monitoring. The dataset contains paired Sentinel-1 and Sentinel-2 Images for 2 locations in Scotland and India. Notably, the cloud regions in the dataset are simulated with a cloud coverage between 10% and 50%. It will inevitably lead to unrealistic representations that cannot generalize to the scenario of real cloud-covered satellite imagery and their spectral characteristics (Ebel et al., 2020).

In addition to the previously mentioned public datasets, there are also several non-public datasets. For example, Enomoto et al. (2017) create a dataset by synthesizing the simulated cloud on the cloud-free images with eight comparatively cloudless WorldView-2 images for learning. Cresson et al. (2019) use Sentinel-2 images acquired over the province of Tuy, Burkina Faso to construct experiments. Gao et al. (2020) collect two simulated datasets with around 35% cloud cover based on Gaofen-2 optical imagery and airborne optical imagery, respectively, and a real dataset based on Sentinel-2 optical imagery. These datasets are relatively small in size and contain a limited number of scenarios. While featuring high resolution imagery, cloudy observations are all simulated.

The majority of datasets containing real-life clouds are based on medium-resolution Sentinel-2 data. It is hard to develop and evaluate the removal of clouds in high resolution imagery with salient structures and abundant textured features. Our Planet-CR dataset aims to advance the task of cloud removal from high resolution imagery by releasing the cloudy and cloud-free PlanetScope data with short time lags in combination with Sentinel-1 SAR data and WorldCover land cover maps. The inclusion of Sentinel-1 SAR data enables the exploration of multi-modal fusion for cloud removal, and the inclusion of WorldCover land cover product enables to disentangle the performance over different land cover types and evaluate the quality of recovered semantic information. While the short revisit time may facilitate to temporal mosaicing, it is not applicable to time-critical applications (Voigt et al., 2007). And when encountering continual cloudy days, cloud-free reference data from an adjacent period is largely unavailable (Xu et al., 2022). It is worth noticing that Sarukkai et al. (2020) train a baseline land classification model and evaluate its accuracy from cloudy, cloud-free, and predicted cloud-free images, respectively, to demonstrate the power of the predicted cloud-free images

for downstream use. However, cloud removal is a pixel-level reconstruction task, an image-level classification task cannot adequately reflect the quality of predicted cloud-free images. Because the correct class can be inferred even if the image is partially occluded (Gu et al., 2022). With our Planet-CR dataset, a pixel-level classification task, i.e. semantic segmentation, can be designed, which will be more suitable for evaluating the power of the cloud removal methods on semantic information recovery.

2.2. Algorithms for Cloud Removal

Cloud removal in optical remote sensing imagery is a long-term research problem. Most early developments address this problem by interpolation (Zhang et al., 2007; Yu et al., 2011), filtering (Mitchell et al., 1977; Liu and Hunt, 1984), or inpainting (Li et al., 2002; Helmer and Ruefenacht, 2005). Currently, deep learning-based methods are gaining considerable attention. They have the potential to solve many of the problems that arise in traditional cloud removal methods and achieve impressive results. For example, Multispectral conditional Generative Adversarial Networks (McGANs) (Enomoto et al., 2017), leveraging the remarkable generative capabilities of conditional Generative Adversarial Networks (cGANs), remove simulated clouds from Worldview-2 imagery by extending the input channels of cGANs to be compatible with multispectral input. Cloud-GAN (Singh and Komodakis, 2018) learns the mapping between cloudy and cloud-free Sentinel-2 imagery using a cyclic consistent generative adversarial network. RSC-Net (Li et al., 2019) estimates the cloud-free output with the contaminated Landsat-8 imagery based on an encoding-decoding framework consisting of multiple residual convolutional layers and residual deconvolutional layers.

As the clouds thicken and the cloud-covered region is dominant, the task of removing the clouds becomes more challenging. A series of work explore the potential of SAR data as auxiliary data for cloud removal in optical imagery. For example, DSen2-CR (Meraner et al., 2020) uses a deep residual neural network to predict the target cloud-free optical image from the concatenation of Sentinel-1 SAR image and Sentinel-2 optical image. Simulation-Fusion GAN (Gao et al., 2020) fuse SAR and corrupted optical imagery with two generative adversarial networks to acquire the cloud-free

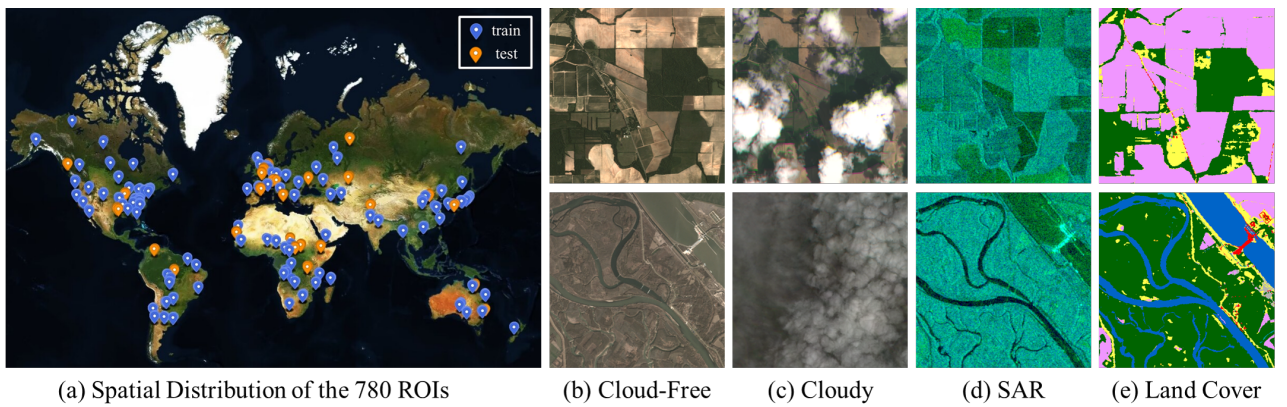


Fig. 1: Visualization of the Planet-CR dataset. (a) Spatial distribution of the 780 AOIs of the Planet-CR dataset. (b) Cloud-free optical observations from PlanetScope. (c) Cloudy optical observations from PlanetScope. (d) SAR observations from Sentinel-1. (e) land cover maps from WorldCover. They are resized to the same size for better view.

results of simulated cloudy Gaofen-2 data and real cloudy Sentinel-2 data. GLF-CR (Xu et al., 2022) incorporates the contribution of Sentinel-1 SAR image in restoring reliable texture details and maintaining global consistency to reconstruct the occluded region of Sentinel-2 optical image. However, these methods are developed on data with relatively low spatial resolutions. The problem of cloud removal in high-resolution imagery remains largely underexplored.

3. Data

3.1. Curation of Planet-CR

To develop the cloud removal methods that are equally applicable to heterogeneous Earth observation data, the Planet-CR dataset curates 780 non-overlapping, highly representative locations of AOIs that are distributed over all continents and meteorological seasons of the globe, as shown in Fig. 1. Each AOI is composed of a quartet of orthorectified, geo-referenced cloudy and cloud-free optical images, as well as the corresponding SAR image and land cover map.

Optical data. The optical data of our dataset originates from the PlanetScope satellite constellation operated by Planet Labs. We gather the cloud-free and cloudy observations from the Level-3B top-of-atmosphere reflectance product, which are radiometrically-, sensor-, and geometrically-corrected. It provides four-band (Blue, Red, Green and Near-Infrared) imagery with a spatial resolution of $3m$. In our dataset, the average time interval between paired cloudy and cloud-free data is 2.8 days. This is shorter than the intra-mission revisiting period of Landsat-8 and Sentinel-2 satellites, and minimizes the amount of land cover change occurring between our paired data. And the cloudy data features a diversity of clouds, ranging from semi-transparent to dense, and from light to heavy cloud covering. In addition to the cloudy and reference cloud-free data, we also collect the cloud masks associated with cloudy PlanetScope images according to the Unusable Data Mask (UDM) assets provided by Planet Labs. UDM masks give information about which pixels in the images are clear or cloudy, permitting a

statistical evaluation of cloud coverage and enabling cloud mask-guided methods to work.

SAR data. The SAR data of our dataset originates from the Sentinel-1 mission operated by the European Space Agency. We gather the Sentinel-1 data with a spatial resolution of $10m$ from the Level-1 Ground Range Detected (GRD) product archived by Google Earth Engine (Gorelick et al., 2017). The measurements are acquired in interferometric wide swath (IW) mode with two polarization channels VV (vertical transmit/vertical receive) and VH (vertical transmit/horizontal receive), which are pre-processed with thermal noise removal, radiometric calibration, terrain correction, and are converted to backscatter coefficients (σ^0) in units of decibels (dB).

Land cover map. The land cover maps of our dataset originates from WorldCover, which is an open-access global land cover product at $10m$ resolution released by the European Space Agency. In this study, we reclassified the data into 6 basic land cover types according to DeepGlobe 2018 (Demir et al., 2018): forest land, rangeland, agriculture land, urban land, barren land and water.

We partition the dataset into train and test splits to allow for direct comparison with future works. A total of 780 AOIs are split into 660 scenes for training and 120 for testing following a random global distribution. To train the deep learning-based methods, we crop each AOI into small patches using slide windows of sensor-specific sizes. Since the spatial resolution of PlanetScope imagery is $3m$, and the spatial resolution of Sentinel-1 imagery as well as WorldCover land cover maps is $10m$, we set the corresponding slide window sizes to 300×300 and 90×90 pixels. For the purpose of uniform distribution over different cloud coverage levels as well as land cover types, we finally select 60,000 quartets of training samples and 3,000 quartets of testing samples. The statistics about cloud coverage and land cover types can be seen in Fig. 2.

3.2. Properties of Planet-CR

High Spatial Resolution. The Planet-CR dataset releases the cloudy and cloud-free PlanetScope data with a spatial

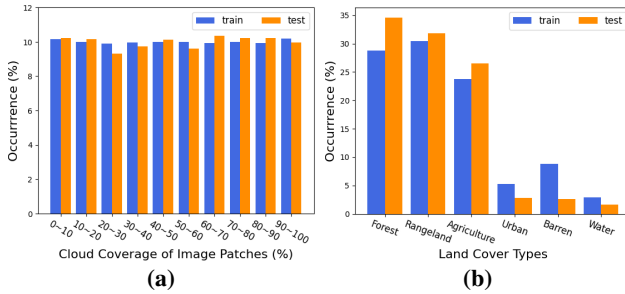


Fig. 2: Statistics of the Planet-CR dataset. (a) Distribution of cloud coverage. (b) Distribution of land cover types.

resolution of 3m. Compared to existing publicly available cloud removal datasets which are mostly built on medium-resolution Landsat-8 data or Sentinel-2 data, our dataset redeems the current lack of cloud removal datasets with high resolution, and advances the task of high-resolution cloud removal that is still under-explored.

Multi-Modal and Multi-Resolution. The inclusion of Sentinel-1 SAR data can provide auxiliary information to promote cloud removal of PlanetScope data. Compared with the existing cloud removal datasets like SEN12MS-CR, which mostly explore the fusion of Sentinel-1 SAR data and Sentinel-2 optical data with the same resolution of 10m, our Planet-CR dataset helps to understand a more practical yet more complex problem, i.e., multi-modal and multi-resolution data fusion based cloud removal.

Information on Land Cover. The inclusion of land cover can disentangle the performance of cloud removal methods over different land cover types on the one hand, and encourages to design a pixel-level classification task to evaluate the power of the cloud removal method in generating semantically meaningful structures on the other.

4. Methodology

4.1. Problem Statement

Given a cloudy image \mathcal{Y} , the task of cloud removal aims to reconstruct a clear image \mathcal{F} revealing the complete information content of the ground scene so that subsequent analysis can be reliably performed. The basic strategy is to deal with the cloud contamination in a single image without additional information, i.e., the problem of **single image Cloud Removal(CR)**, which can be formulated as:

$$\mathcal{F} = \text{CR}(\mathcal{Y}) \quad (1)$$

It is a highly ill-posed problem, usually solved under the assumption that the cloud-contaminated regions have similar spectral/geometrical characteristics to the remaining parts of the image. However, when it comes to the areas with high-frequency texture or different land cover types, the reconstruction performance cannot be guaranteed. Many studies resort to SAR images that are cloud-penetrable and inherently reflect the geometrical shapes of ground objects as an a priori assumption to reduce the ill-posedness. Thus, the problem of **Multi-Modal data Fusion based Cloud**

Removal (MMF-CR) is introduced. It restores the clear image from a cloudy image and the corresponding SAR image \mathcal{S} , formulated as:

$$\mathcal{F} = \text{MMF-CR}(\mathcal{Y}_\Omega, \mathcal{S}_\Omega) \quad (2)$$

where Ω indicates the same spatial domain shared by the cloudy image and the corresponding SAR image. The SAR image guides most MMF-CR methods to restore the cloud-free image from pixel-to-pixel aligned cloudy and SAR images. However, the geo-referenced cloudy images captured by Planet satellites and SAR images captured by Sentinel-1 satellites in the Planet-CR dataset do not meet the assumption of pixel-to-pixel alignment, mainly caused by resolution difference, field-of-view mismatch and disparity. The problem of **Multi-Modal and multi-Resolution data Fusion based Cloud Removal**(MMRF-CR) is thus introduced:

$$\mathcal{F} = \text{MMRF-CR}(\mathcal{Y}_{\Omega_y}, \mathcal{S}_{\Omega_s} | \mathcal{M}) \quad (3)$$

where Ω_y and Ω_s respectively denote the spatial domain of the cloudy image and the SAR image, and $\mathcal{M} : \Omega_s \rightarrow \Omega_y$ denotes the pixel-level correspondence mapping operator. To solve the problem of MMRF-CR, it is required to precisely align the cloudy and SAR images for the cloud removal process.

4.2. Align-CR Network

The proposed network, called Align-CR, adopts a two-stream architecture to compensate for the missing information in cloudy regions using ancillary SAR image, as shown in Fig. 3. Since the SAR image has a lower resolution, an upsampling operator is firstly employed to map it to the same resolution as the optical image. Then, the cloudy optical image and the upsampled SAR image are passed through their respective feature extraction blocks to extract modality-specific features F_{opt}^0 and F_{sar}^0 . After that, F_{opt}^0 and F_{sar}^0 are fed into D AlignFuse blocks to obtain knowledgeable features with comprehensive information. The AlignFuse block performs alignment and fusion sequentially in the feature space.

$$\hat{F}_{sar}^i = H_{\text{Align}}(F_{opt}^i, F_{sar}^i), \quad (4)$$

$$F_{opt}^{i+1}, F_{sar}^{i+1} = H_{\text{fuse}}(F_{opt}^i, \hat{F}_{sar}^i), \quad (5)$$

where $H_{\text{Align}}(\cdot)$ and $H_{\text{fuse}}(\cdot)$ denote the functions of the alignment block and the fusion block, respectively, and the details are shown in Sec. 4.2.1 and 4.2.2. Finally, all intermediate features $\{F_{opt}^i\}_{i=1}^D$ are aggregated to reconstruct the high-quality cloud-free image.

4.2.1. Alignment Block

Ideally, the task of MMRF-CR can be considered as a two-step task that aligns the multi-modal and multi-resolution data first and reconstruct the clear image following Eq. 2 later. However, explicit pixel-to-pixel alignment to ensure that the same pixels in the SAR image and the cloudy image reflect the same ground target is very hard

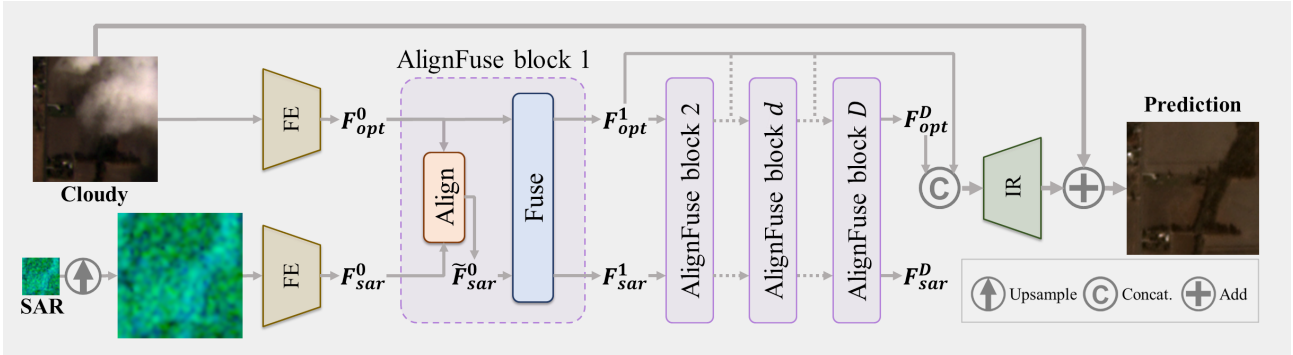


Fig. 3: Overview of the proposed Align-CR method. An upsampling operator is firstly employed to map the SAR image to the same resolution as the optical image. Then, the cloudy optical image and the upsampled SAR image are passed through their respective feature extraction (FE) blocks to extract modality-specific features. After that, the features are fed into D AlignFuse blocks to obtain knowledgeable features with comprehensive information. The AlignFuse block performs alignment and fusion sequentially in the feature space. Finally, the output of all AlignFuse blocks are concatenated and fed to the image reconstruction (IR) block to restore the high-quality cloud-free image.

to achieve in our case. On the one hand, sharp edges in the high-resolution optical image cannot be exactly aligned with blurry edges in the low-resolution SAR image. On the other hand, for non-co-orbital satellite data, it is very difficult to resolve the unalignment caused by field-of-view mismatch and disparity. Moreover, the occlusions in the cloudy images complicates the pixel-to-pixel alignment. Therefore, we implicitly learn the alignment process for cloud-free image reconstruction. In this paper, we resort to the deformable convolution to align the SAR features to the optical features. Given two features to be aligned as input, i.e., F_{opt}^i and F_{sar}^i , $i = 0, \dots, D - 1$, The core to solve feature misalignment is to predict the offset with an offset prediction module,

$$\Delta p^i = H_{\text{offset}}(F_{opt}^i, F_{sar}^i), \quad (6)$$

where H_{offset} denotes the function of the offset prediction module, which can be implemented by general convolutional layers. With the predicted offset, the SAR feature can be warped to the optical feature using the deformable convolution (DConv),

$$\hat{F}_{sar}^i = \text{DConv}(F_{sar}^i, \Delta p^i), \quad (7)$$

Specifically, we adopt the Pyramid, Cascading and Deformable convolutions (PCD) (Wang et al., 2019) for the alignment process. It performs the alignment in a pyramid structure, i.e., aligning the features in lower scales with coarse estimations first and propagating the aligned features and learned offsets to higher scales to refine the estimations later. Embedding it into the network, the network's ability to model transformations can be enhanced.

4.2.2. Fusion Block

The aligned features, i.e., F_{opt}^i and \hat{F}_{sar}^i , are then fed into the fusion block for the transfer of complementary information. Similar to our prior work (Xu et al., 2022), we exploit the power of SAR information from two aspects: global fusion, to guide the global interactions among all

local optical windows; local fusion, to transfer the SAR feature corresponding to cloudy areas to compensate for the missing information. Specifically, each fusion block contains an adapted SAR-guided global context interaction (SGCI) block followed by a SAR-based local feature compensation (SLFC) block. To reduce the complexity of the SGCI block, instead of adding a Swin Transformer layer (STL) (Liu et al., 2021) after each convolutional layer in the dense connected layers, we only add a STL after the convolutional layer in the local feature fusion of the residual dense block (RDB) (Zhang et al., 2020) for cross-window feature interaction.

4.2.3. Loss Function

We train the Align-CR network by minimizing the difference between the output of network y and the cloud-free image \hat{y} temporally close to the input cloudy image. Though the Planet-CR has avoided the surface changes that may appear between the acquisitions of cloudy and cloud-free images as much as possible through short time lag for data collection, there are some inevitable nuisances determined by the sunlight condition, acquisition geometry, humidity, pollution, change of landscape, etc (Xu et al., 2022). In this paper, we use the Charbonnier loss (Lai et al., 2017) which can better handles outlier for training, and extra constraints on cloudy regions are applied,

$$\mathcal{L} = (1 + w\mathbf{M}) \odot ((y - \hat{y})^2 + \epsilon^2)^\alpha \quad (8)$$

where \odot denotes Hadamard product operator, w denotes the extra weight for cloudy regions, \mathbf{M} denotes the cloudy mask, ϵ and α are constants.

5. Evaluations

5.1. Experimental Settings

Preprocessing. Before the PlanetScope and Sentinel-1 data are fed into the neural networks, we apply value clipping to eliminate a small number of anomalous pixels and data scaling to improve the stability of the neural networks. We

Table 2

Quantitative results of visual recovery quality over different land cover types.

(a) results on objective assessment metrics, MAE and PSNR, to quantify the prediction error

	per class MAE ↓						MAE↓	PSNR↑
	Forest	Rangeland	Agriculture	Urban	Barren	Water		
McGAN	0.0321	0.0417	0.0497	0.0492	0.0507	0.0442	0.0425	26.4273
SpA GAN	0.0358	0.0376	0.0393	0.0444	0.0423	0.0425	0.0381	26.1448
SAR-Opt-cGAN	0.0300	0.0296	0.0331	0.0352	0.0344	0.0414	0.0323	28.2106
DSen2-CR	0.0289	0.0293	0.0311	0.0352	0.0340	0.0353	0.0298	28.7832
GLF-CR	0.0231	0.0257	0.0293	0.0329	0.0322	0.0274	0.0256	29.9848
Ours (wo/ SAR)	0.0261	0.0259	0.0296	0.0321	0.0315	0.0369	0.0272	29.6859
Ours (wo/ Align)	0.0238	0.0251	0.0282	0.0318	0.0311	0.0311	0.0255	30.0107
Ours (Align-CR)	0.0219	0.0243	0.0277	0.0324	0.0311	0.0257	0.0238	30.4785

(b) results on subjective assessment metrics, SAM and SSIM, to quantify spectral and structural similarity

	per class SAM ↓						SAM↓	SSIM↑
	Forest	Rangeland	Agriculture	Urban	Barren	Water		
McGAN	9.5005	12.1237	13.4662	14.6771	14.4427	15.6362	12.2471	0.7975
SpA GAN	8.9910	8.7126	8.4814	10.1953	9.6112	18.1517	9.2522	0.8181
SAR-Opt-cGAN	7.4595	6.4506	6.7722	8.1655	7.1440	11.0905	7.2188	0.8602
DSen2-CR	7.1437	6.5581	6.3116	7.7517	7.2008	9.7014	6.6527	0.8806
GLF-CR	5.7830	5.7131	5.7403	7.8324	7.0525	9.7931	5.6189	0.9063
Ours (wo/ SAR)	7.0319	6.2599	6.3504	7.6640	7.0522	10.1132	6.5402	0.8930
Ours (wo/ Align)	6.0453	5.7382	5.7558	7.5235	6.8470	9.6844	5.7816	0.9021
Ours (Align-CR)	5.5766	5.5408	5.6306	7.8660	7.0693	9.5205	5.4183	0.9124

clip the values of all bands of the PlanetScope data to [0, 10,000] and divide by 10,000 for all bands. We clip the VV and VH polarizations of the Sentinel-1 data to values [-25, 0] and [-32.5, 0], respectively, and rescale them to the range [0, 1]. All experiments in this paper use these preprocessing steps, following previous best practices (Meraner et al., 2020; Ebel et al., 2020).

Implementation Details. The proposed Align-CR network is implemented using Pytorch and trained on 2 NVIDIA Geforce RTX 3090 GPUs with a batch size of 12. During training, we randomly crop the samples into 160×160 patches. The Adam optimizer is used and the maximum epoch of training iterations is set to 30. The learning rate is set to 10^{-4} for the whole network except for the Alignment blocks where the learning rate is set to a smaller value of 10^{-5} . And the learning rates decays by 50% every 5 epochs after the first 10 epochs. For the network architecture, the upsampling operator adopts the nearest neighbor interpolation and the number of the AlignFuse blocks D is set to 6. For the loss function, w , ϵ and α is set to 5, 10^{-3} and 0.45, respectively.

Baselines In this paper, we compare the proposed method with 5 baseline methods on the Planet-CR dataset with the proposed data splits, including the single image cloud removal methods, McGAN (Enomoto et al., 2017) and SpA GAN (Pan, 2020), and the multi-modal data fusion based cloud removal methods, SAR-Opt-cGAN (Grohnfeldt et al., 2018), DSen2-CR (Meraner et al., 2020) and GLF-CR (Xu et al., 2022). Since existing multi-modal data fusion based

cloud removal methods require the input SAR images to be of the same spatial resolution as the input optical images, upsampling the SAR images in the Planet-CR dataset is necessary for these algorithms to work properly. Here, all multi-modal data fusion based cloud removal methods utilize the SAR images upsampled by the nearest neighbor interpolation as input. Moreover, to determine the benefits of including auxiliary low-resolution SAR images, we train the Align-CR network without use of the SAR images, denoted as w/o SAR. And to validate the superiority of Align-CR in integrating multi-modal and multi-resolution information, we train the Align-CR network by removing the Alignment blocks in the AlignFuse blocks, denoted as w/o Align.

5.2. Evaluation of Visual Recovery Quality

To evaluate the quality of the reconstructed images in terms of generating visually pleasing textures, we report mean absolute error (MAE) and peak signal-to-noise ratio (PSNR) to objectively quantify the prediction error, and spectral angle mapper (SAM) and the structural similarity index measure (SSIM) to subjectively measure the quality of reconstructed images from spectral similarity and structural similarity, respectively. Notably, with the benefit of the land cover annotations, we disentangle the performance of cloud removal methods over different land cover types by pixel-wise MAE and SAM metrics, as shown in Tab. 2. And we choose two scenes to qualitatively evaluate visual recovery quality, as shown in Fig. 4. We can see that the methods McGAN, SpA GAN and SAR-Opt-cGAN, which were developed on relatively small datasets with geographically and

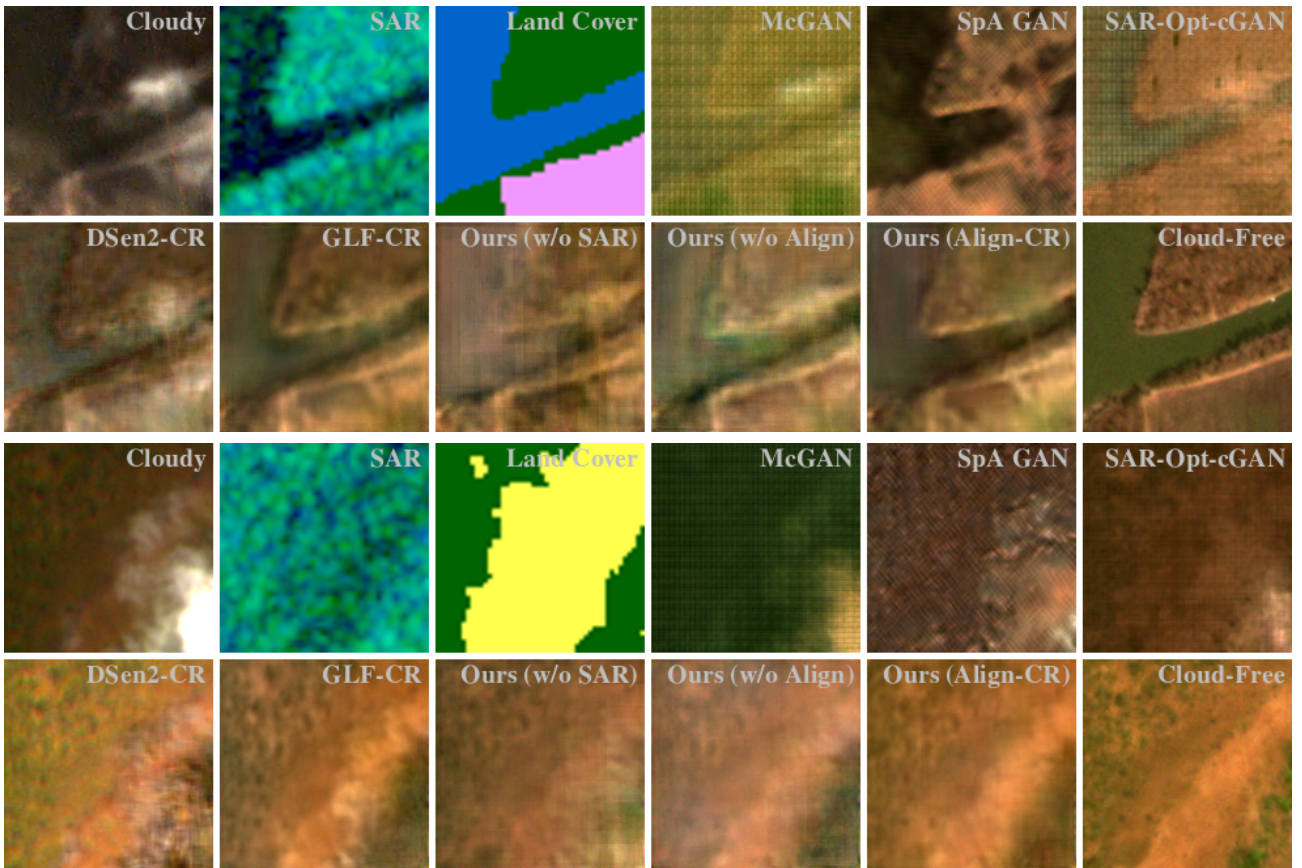


Fig. 4: Qualitative results of visual recovery quality for two different samples. For each sample, from top-left to bottom-right are respectively the cloudy image, the SAR image, the land cover map, the results from McGAN, SpA GAN, SAR-Opt-cGAN, DSen2-CR, GLF-CR, w/o SAR, w/o Align, Align-CR, and the cloud-free image.

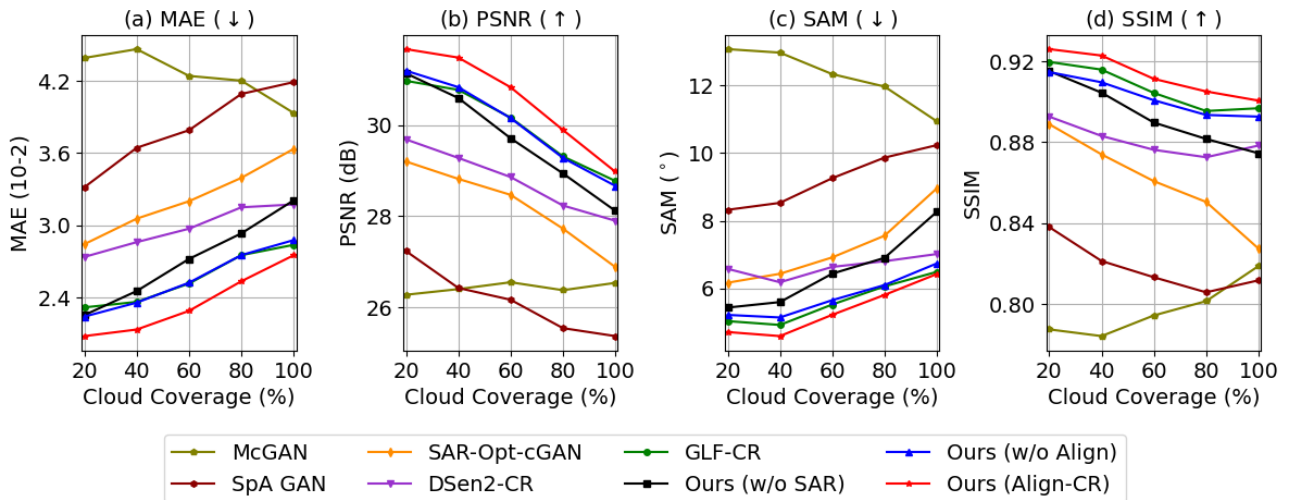


Fig. 5: Quantitative results of visual recovery quality over different cloud cover levels in terms of the MAE, PSNR, SAM, and SSIM quality metrics.

topographically homogeneous data, perform poorly in terms of generalizability on our Planet-CR dataset. Their results have relatively limited spectral fidelity. It indicates the need to take the point of global distribution into consideration when creating a practical dataset. Our method achieves the best performance overall, which can restore images with

more details and fewer artifacts. It indicates the effectiveness and superiority of our method on restoring cloud-free images. Moreover, we compare the results over different land cover types. We can find that removing clouds over urban land that has highly complex geometrical structures is more challenging than others. And we can find that the results over water do not perform well on SAM but relatively well on

Table 3

The performance of semantic recovery quality over different cloud cover levels.

	0~20%		20~40%		40~60%		60~80%		80~100%		Overall	
	mIoU	PA	mIoU	PA	mIoU	PA	mIoU	PA	mIoU	PA	mIoU	PA
Cloud-Free	44.63	62.68	43.66	65.44	41.85	64.40	40.58	64.16	42.98	66.70	43.24	64.66
Cloudy	18.89	34.08	13.26	24.84	10.24	19.27	8.62	16.21	7.89	13.00	11.72	21.46
McGAN	17.63	35.13	17.84	34.08	15.51	31.99	15.30	32.06	12.52	39.88	16.62	34.64
SpA GAN	24.07	41.37	21.93	41.94	17.31	37.66	14.03	35.18	10.44	28.99	16.15	36.97
SAR-Opt-cGAN	12.78	31.43	11.25	28.84	9.85	28.59	9.10	28.99	9.15	28.09	10.44	29.20
DSen2-CR	33.11	43.96	30.17	39.03	26.05	37.73	22.94	35.91	23.10	41.92	28.11	39.72
GLF-CR	33.99	47.66	31.54	44.96	27.02	40.90	22.44	39.49	22.95	45.19	28.75	43.63
Ours (w/o SAR)	31.85	45.72	25.14	39.83	20.91	37.34	16.95	37.02	11.58	41.02	20.97	40.20
Ours (w/o Align)	33.80	46.94	30.85	41.61	26.76	38.97	22.39	38.69	23.94	44.67	28.47	42.19
Ours (Align-CR)	37.32	51.16	32.90	45.40	28.93	43.22	24.17	42.37	23.43	46.69	30.51	45.78

MAE. It indicates the challenge in maintaining the spectral fidelity over water.

To determine what contributes to the superior performance of the proposed method, we analyze the effectiveness of each component by comparing the proposed method with its variants, i.e., w/o SAR and w/o Align. We can find that w/o SAR tends to generate undesirable artifacts for cloud-covered regions due to the lack of ground information. While Align-CR exploits the geometrical information embedded in the SAR images, which can reconstruct the ground object. We further compare the cloud removal performance of w/o Align to Align-CR. When the Alignment blocks are removed, the gain of integrating low-resolution SAR information is reduced. In regards to the misalignment, such as the river border in the first sample and the junction of different land cover types in the second sample in Fig. 4, w/o Align tends to generate blurring artifacts, while the reconstructed results of Align-CR have sharper edges. It demonstrates the superiority of our proposed Align-CR method in integrating multi-modal and multi-resolution information.

We further assess the reconstruction performance on different cloud cover levels, as shown in Fig. 5. The performance of all methods, except McGAN, decreases roughly as the percentage of cloud cover increases. Among them, the performance of the methods with the benefit of SAR images degrades more slowly than the one without, since the utilization of SAR images can alleviate the decline to some extent. Align-CR performs favorably when compared with all baseline methods. When the Alignment blocks are removed, w/o Align behaves very similarly to GLF-CR, while GLF-CR contains more Transformer layers for global fusion and thus performs slightly better in terms of SSIM. Our method Align-CR, which aligns the multi-modal and multi-resolution data during the reconstruction process, can better exploit the power of SAR information. It steadily outperforms w/o Align on all cloud cover levels.

5.3. Evaluation of Semantic Recovery Quality

In addition to evaluating in generating visually pleasing textures, we further evaluate in generating semantically meaningful structures, where the semantic information is important for future analytical applications. In this paper, we

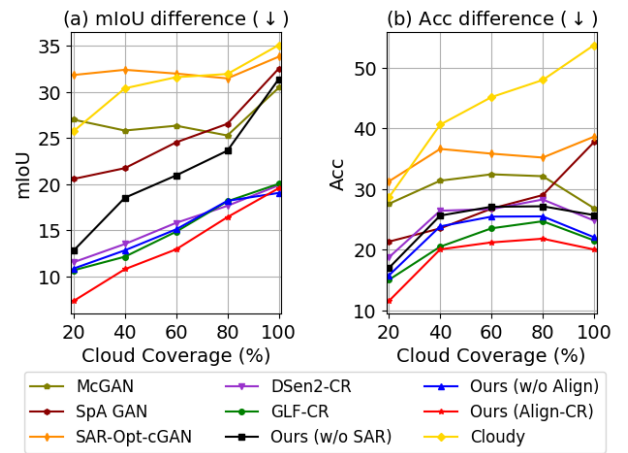


Fig. 6: The discrepancy between the results with the cloud-free images as input and the results with the predicted cloud-free images as well as cloudy images as input.

evaluate the quality of the recovered semantic information through a well-established land cover semantic segmentation model. Using the cloud-free PlanetScope images and associated land cover annotations, we train a land cover semantic segmentation model with the same data splits adopted for the experiments on cloud removal. The model is based on DeepLabv3plus (Chen et al., 2018) with ResNet-50 (He et al., 2016) as the backbone network. With the cloud-free images, cloudy images and predicted cloud-free images from benchmarked models as inputs respectively, we evaluate the performance of the trained land cover semantic segmentation model in predicting the correct class of each pixel. Ideally, the results with the predicted images as input should be as consistent as possible with the results with the cloud-free images as input, i.e., the closer they are to the results with the cloud-free images as input, the better the corresponding cloud removal method performs in terms of semantic recovery. We report the mean intersection over union (mIoU) and pixel accuracy (PA) over varying levels of cloud cover in Tab. 3, where mIoU can better deal with the class imbalance issue. Additionally, we show the discrepancy between the results with the cloud-free images as input

and the results with the predicted cloud-free images as well as cloudy images as input in Fig. 6.

Clearly, the existence of clouds deteriorates the semantic analysis, and the degradation is more severe when the cloud cover level is higher. The benchmarked cloud removal models can to some extent counteract the degradation, in which Align-CR generally performs the best. Notably, we can observe that the trained land cover semantic segmentation model performs better with the predicted images of McGAN and SpA GAN as input than with the predicted images of SAR-Opt-cGAN as input. While SAR-Opt-cGAN performs better than McGAN and SpA GAN in terms of all visual quality metrics, as shown in Fig. 5. It indicates that the metrics for measuring the visual recovery quality can not adequately reflect the performance of cloud removal methods in terms of semantic recovery. We can also find this by comparing the performance of w/o Align and Align-CR. Align-CR steadily outperforms w/o Align on all cloud cover levels in terms of all visual quality metrics. However, it does not perform as well as w/o Align on the images with cloud cover 80% to 100% in terms of mIoU. What's more, we can find that its performance in terms of mIoU is more superior to that of w/o Align when more prior information from cloud-free regions is available, since there is more information available for alignment.

6. Discussion

Due to the shortcomings in semantic annotations, the vast majority of current studies quantify the goodness of cloud removal methods exclusively by metrics that assess the visual similarity between two images. Towards the direction of boosting the performance on the visual metrics, most methods use the the loss functions that are constructed based on these metrics to guide the training of cloud removal models, e.g., L1 loss function computes the mean absolute error (Xu et al., 2022). It will motivate the predicted cloud-free image to move towards over-smoothness and lead to the loss of semantic information. As we have validated in Sec. 5.3, the current visual metrics cannot adequately evaluate the quality of recovered semantic information. Though our method performs the best in terms of semantic recovery, there is still a large gap between its predicted cloud-free images and real cloud-free images. Therefore, it is very important for the cloud removal field to design a loss function that can guide the recovery of semantic information. Future work could consider the correlation between cloud removal and downstream task, and design the loss function by balancing the semantic context and image details to guide the reconstruction process.

7. Conclusion

We introduce Planet-CR, a multi-modal and multi-resolution dataset for cloud removal in high-resolution optical remote sensing imagery. We offer the dataset as open-source with the purpose of developing new cloud removal

approaches towards high resolution by integrating multi-modal and multi-resolution information. We address the problem of multi-modal and multi-resolution data fusion based cloud removal by proposing a novel method called Align-CR, which implicitly aligns the feature maps during the reconstruction process to compensate for the misalignment between the multi-modal and multi-resolution data. The experimental results in both visual recovery quality and semantic recovery quality demonstrate the effectiveness and superiority of the proposed method than the existing representative cloud removal methods. We believe the Planet-CR dataset will prove beneficial for the community and our evaluations provide valuable directions for future research.

Acknowledgements

The work of W. Yang is supported by the National Natural Science Foundation of China (NSFC) Regional Innovation and Development Joint Fund (No. U22A2010). The work of X. Zhu is jointly supported by the European Research Council (ERC) under the European Union's Horizon 2020 research and innovation programme (grant agreement No. [ERC-2016-StG-714087], Acronym: *So2Sat*), by the Helmholtz Association through the Framework of the Helmholtz Excellent Professorship "Data Science in Earth Observation - Big Data Fusion for Urban Research"(grant number: W2-W3-100), by the German Federal Ministry of Education and Research (BMBF) in the framework of the international future AI lab "AI4EO – Artificial Intelligence for Earth Observation: Reasoning, Uncertainties, Ethics and Beyond" (grant number: 01DD20001) and by German Federal Ministry for Economic Affairs and Climate Action in the framework of the "national center of excellence ML4Earth" (grant number: 50EE2201C).

References

- Atwood, D., Garron, J., 2013. Addressing three fallacies about synthetic aperture radar. *Eos, Transactions American Geophysical Union* 94, 471–472.
- Chen, L.C., Zhu, Y., Papandreou, G., Schroff, F., Adam, H., 2018. Encoder-decoder with atrous separable convolution for semantic image segmentation, in: European Conference on Computer Vision, pp. 801–818.
- Cornebise, J., Oršolić, I., Kalaitzis, F., 2022. Open high-resolution satellite imagery: The worldstrat dataset—with application to super-resolution. *arXiv:2207.06418*.
- Cresson, R., Ienco, D., Gaetano, R., Ose, K., Minh, D.H.T., 2019. Optical image gap filling using deep convolutional autoencoder from optical and radar images, in: IEEE International Geoscience and Remote Sensing Symposium, pp. 218–221.
- Cresson, R., Narçón, N., Gaetano, R., Dupuis, A., Tanguy, Y., May, S., Commandre, B., 2022. Comparison of convolutional neural networks for cloudy optical images reconstruction from single or multitemporal joint sar and optical images. *arXiv:2204.00424*.
- Czerkawski, M., Upadhyay, P., Davison, C., Werkmeister, A., Cardona, J., Atkinson, R., Michie, C., Andonovic, I., Macdonald, M., Tachtatzis, C., 2022. Deep internal learning for inpainting of cloud-affected regions in satellite imagery. *Remote Sensing* 14.
- Dai, J., Qi, H., Xiong, Y., Li, Y., Zhang, G., Hu, H., Wei, Y., 2017. Deformable convolutional networks, in: IEEE International Conference on Computer Vision, pp. 764–773.

Demir, I., Koperski, K., Lindenbaum, D., Pang, G., Huang, J., Basu, S., Hughes, F., Tuia, D., Raskar, R., 2018. Deepglobe 2018: A challenge to parse the earth through satellite images, in: IEEE Conference on Computer Vision and Pattern Recognition Workshops, pp. 172–181.

Duan, C., Li, R., 2020. Multi-head linear attention generative adversarial network for thin cloud removal. arXiv:2012.10898 .

Ebel, P., Meraner, A., Schmitt, M., Zhu, X.X., 2020. Multisensor data fusion for cloud removal in global and all-season sentinel-2 imagery. *IEEE Transactions on Geoscience and Remote Sensing* 59, 5866–5878.

Ebel, P., Xu, Y., Schmitt, M., Zhu, X.X., 2022. Sen12ms-cr-ts: A remote-sensing data set for multimodal multitemporal cloud removal. *IEEE Transactions on Geoscience and Remote Sensing* 60, 1–14. doi:10.1109/GRS.2022.3146246.

Enomoto, K., Sakurada, K., Wang, W., Fukui, H., Matsuoka, M., Nakamura, R., Kawaguchi, N., 2017. Filmy cloud removal on satellite imagery with multispectral conditional generative adversarial nets, in: IEEE Conference on Computer Vision and Pattern Recognition Workshops, pp. 48–56.

Fisher, A., Flood, N., Danaher, T., 2016. Comparing landsat water index methods for automated water classification in eastern australia. *Remote Sensing of Environment* 175, 167–182.

Gao, J., Yuan, Q., Li, J., Zhang, H., Su, X., 2020. Cloud removal with fusion of high resolution optical and sar images using generative adversarial networks. *Remote Sensing* 12, 191.

Gorelick, N., Hancher, M., Dixon, M., Ilyushchenko, S., Thau, D., Moore, R., 2017. Google Earth Engine: Planetary-scale geospatial analysis for everyone. *Remote Sensing of Environment* 202, 18–27.

Grohnfeldt, C., Schmitt, M., Zhu, X., 2018. A conditional generative adversarial network to fuse sar and multispectral optical data for cloud removal from sentinel-2 images, in: IEEE International Geoscience and Remote Sensing Symposium, pp. 1726–1729.

Gu, Z., Ebel, P., Yuan, Q., Schmitt, M., Zhu, X.X., 2022. Explicit haze & cloud removal for global land cover classification, in: IEEE Conference on Computer Vision and Pattern Recognition Workshops.

He, K., Zhang, X., Ren, S., Sun, J., 2016. Deep residual learning for image recognition, in: IEEE Conference on Computer Vision and Pattern Recognition, pp. 770–778.

Helmer, E.H., Ruefenacht, B., 2005. Cloud-free satellite image mosaics with regression trees and histogram matching. *Photogrammetric Engineering & Remote Sensing* 71, 1079–1089.

Kondmann, L., Toker, A., Rußwurm, M., Camero, A., Peressutti, D., Milcinski, G., Mathieu, P.P., Longepie, N., Davis, T., Marchisio, G., Leal-Taixé, L., Zhu, X., 2021. Denethor: The dynamicearthnet dataset for harmonized, inter-operable, analysis-ready, daily crop monitoring from space, in: Neural Information Processing Systems Track on Datasets and Benchmarks.

Lai, W.S., Huang, J.B., Ahuja, N., Yang, M.H., 2017. Deep laplacian pyramid networks for fast and accurate super-resolution, in: IEEE Conference on Computer Vision and Pattern Recognition, pp. 5835–5843.

Li, J., Wu, Z., Hu, Z., Li, Z., Wang, Y., Molinier, M., 2021. Deep learning based thin cloud removal fusing vegetation red edge and short wave infrared spectral information for sentinel-2a imagery. *Remote Sensing* 13, 157.

Li, M., Liew, S.C., Kwoh, L.K., 2002. Generating "cloud free" and "cloud-shadow free" mosaic for spot panchromatic images, in: IEEE International Geoscience and Remote Sensing Symposium, pp. 2480–2482.

Li, W., Li, Y., Chen, D., Chan, J.C.W., 2019. Thin cloud removal with residual symmetrical concatenation network. *ISPRS Journal of Photogrammetry and Remote Sensing* 153, 137–150.

Lima, T.A., Beuchle, R., Langner, A., Grecchi, R.C., Griess, V.C., Achard, F., 2019. Comparing sentinel-2 msi and landsat 8 oli imagery for monitoring selective logging in the brazilian amazon. *Remote Sensing* 11, 961.

Lin, D., Xu, G., Wang, X., Wang, Y., Sun, X., Fu, K., 2019. A remote sensing image dataset for cloud removal. arXiv:1901.00600 .

Liu, Z., Hunt, B.R., 1984. A new approach to removing cloud cover from satellite imagery. *Computer Vision, Graphics, and Image Processing* 25, 252–256.

Liu, Z., Lin, Y., Cao, Y., Hu, H., Wei, Y., Zhang, Z., Lin, S., Guo, B., 2021. Swin transformer: Hierarchical vision transformer using shifted windows, in: IEEE International Conference on Computer Vision, pp. 10012–10022.

Meraner, A., Ebel, P., Zhu, X.X., Schmitt, M., 2020. Cloud removal in sentinel-2 imagery using a deep residual neural network and sar-optical data fusion. *ISPRS Journal of Photogrammetry and Remote Sensing* 166, 333–346.

Mitchell, O., Delp, E.J., Chen, P.L., 1977. Filtering to remove cloud cover in satellite imagery. *IEEE Transactions on Geoscience Electronics* 15, 137–141.

Nagadze, F., Mpakairi, K.S., Kavhu, B., Ndaimani, H., Maremba, M.S., 2020. Exploring the utility of sentinel-2 msi and landsat 8 oli in burned area mapping for a heterogenous savannah landscape. *PLoS ONE* 15, 1–13.

Pan, H., 2020. Cloud removal for remote sensing imagery via spatial attention generative adversarial network. arXiv:2009.13015 .

PBC, P.L., 2018–. Planet application program interface: In space for life on earth. URL: <https://api.planet.com>.

Requena-Mesa, C., Benson, V., Reichstein, M., Runge, J., Denzler, J., 2021. Earthnet2021: A large-scale dataset and challenge for earth surface forecasting as a guided video prediction task., in: Proceedings of the IEEE Conference on Computer Vision and Pattern Recognition, pp. 1132–1142.

Rogan, J., Franklin, J., Roberts, D.A., 2002. A comparison of methods for monitoring multitemporal vegetation change using thematic mapper imagery. *Remote Sensing of Environment* 80, 143–156.

Sarukkai, V., Jain, A., Uzkent, B., Ermon, S., 2020. Cloud removal in satellite images using spatiotemporal generative networks, in: IEEE Winter Conference on Applications of Computer Vision, pp. 1785–1794.

Singh, P., Komodakis, N., 2018. Cloud-gan: Cloud removal for sentinel-2 imagery using a cyclic consistent generative adversarial networks, in: IEEE International Geoscience and Remote Sensing Symposium, pp. 1772–1775.

Voigt, S., Kemper, T., Riedlinger, T., Kiefl, R., Scholte, K., Mehl, H., 2007. Satellite image analysis for disaster and crisis-management support. *IEEE Transactions on Geoscience and Remote Sensing* 45, 1520–1528.

Wang, X., Chan, K.C., Yu, K., Dong, C., Loy, C.C., 2019. Edvr: Video restoration with enhanced deformable convolutional networks, in: IEEE Conference on Computer Vision and Pattern Recognition.

Xia, G.S., Bai, X., Ding, J., Zhu, Z., Belongie, S., Luo, J., Datcu, M., Pelillo, M., Zhang, L., 2018. Dota: A large-scale dataset for object detection in aerial images, in: IEEE Conference on Computer Vision and Pattern Recognition, pp. 3974–3983.

Xiong, Z., Zhang, F., Wang, Y., Shi, Y., Zhu, X.X., 2022. Earthnets: Empowering ai in earth observation. arXiv:2210.04936 .

Xu, F., Shi, Y., Ebel, P., Yu, L., Xia, G.S., Yang, W., Zhu, X.X., 2022. Glf-cr: Sar-enhanced cloud removal with global-local fusion. *ISPRS Journal of Photogrammetry and Remote Sensing* 192, 268–278.

Yu, C., Chen, L., Su, L., Fan, M., Li, S., 2011. Kriging interpolation method and its application in retrieval of modis aerosol optical depth, in: International Conference on Geoinformatics, pp. 1–6.

Yuan, Q., Shen, H., Li, T., Li, Z., Li, S., Jiang, Y., Xu, H., Tan, W., Yang, Q., Wang, J., et al., 2020. Deep learning in environmental remote sensing: Achievements and challenges. *Remote Sensing of Environment* 241, 111716.

Zanaga, D., Van De Kerchove, R., De Keersmaecker, W., Souverijns, N., Brockmann, C., Quast, R., Wevers, J., Grosu, A., Paccini, A., Vergnaud, S., et al., 2021. Esa worldcover 10 m 2020 v100 .

Zhang, C., Li, W., Travis, D., 2007. Gaps-fill of slc-off landsat etm+ satellite image using a geostatistical approach. *International Journal of Remote Sensing* 28, 5103–5122.

Zhang, Y., Tian, Y., Kong, Y., Zhong, B., Fu, Y., 2020. Residual dense network for image restoration. *IEEE Transactions on Pattern Analysis and Machine Intelligence* 43, 2480–2495.